Journal of the Optical Society of Korea
Vol. 20, No. 6, December 2016, pp. 733-738

ISSN: 1226-4776(Print) / ISSN: 2093-6885(Online)
DOI: https://doi.org/10.3807/JOSK.2016.20.6.733

# Analysis on Transition between Index- and Bandgap-guided Modes in Photonic Crystal Fiber

**Kee Suk Hong[1], Sun Do Lim[1,3]*, Hee Su Park[2], and Seung Kwan Kim[1,3]**

[1]*Division of Physical Metrology, Korea Research Institute of Standards and Science, Daejeon 34113, Korea*
[2]*Division of Convergence Technology, Korea Research Institute of Standards and Science, Daejeon 34113, Korea*
[3]*Science of Measurement, Korea University of Science and Technology, Daejeon 34113, Korea*

(Received June 14, 2016 : revised August 10, 2016 : accepted October 11, 2016)

We calculate optical properties of guided modes of a hybrid-guiding photonic crystal fiber. The design and modeling of such hybrid-guiding PCF is made by replacing air holes with inserts of high refractive index material layer by layer in order. The optical properties such as mode intensity profile, mode dispersion, optical birefringence, confinement loss, and chromatic dispersion during transition of the guiding mechanism are analyzed and discussed. The guided modes in the hybrid-guiding region are also compared with those of reference index-guiding and bandgap-guiding photonic crystal fibers.

*Keywords* : Photonic crystal fibers, Photonic bandgap fibers, Numerical modeling, Fiber properties
*OCIS codes* : (060.5295) Photonic crystal fibers; (060.2270) Fiber characterization; (060.2400) Fiber properties

## I. INTRODUCTION

Photonic crystal fibers (PCFs) have been a subject of intensive research over the past twenty years because they provide enhanced optical properties required by new emerging applications. The optical properties that have been emphasized in the literature are endlessly single-mode operation, large mode area, giant nonlinearity, ultra-large birefringence, and ultra-flatten dispersion [1-7]. The presence of air-holes in the fiber greatly widens the range of waveguide parameters, thereby facilitating different guiding mechanisms such as index-guiding, bandgap-guiding, and hybrid-guiding. The index-guiding PCF delivers light by the modified total internal reflection (M-TIR) similar to conventional fibers, having in mind that the effective cladding index is lower than that of the core. The aforementioned amazing optical properties are mainly related to the index-guiding PCF. Unlike the index-guiding PCF, the bandgap-guiding PCF has a higher effective cladding index than the core. In the fiber, the existence of the photonic bandgap in the cladding makes it possible to confine light in the core with low transmission loss for a finite spectral window. All-solid photonic bandgap fiber (ASPBGF) is a type of bandgap-guiding PCF. This has been made of high refractive index material (HRIM) inserts embedded in a PCF preform or filled into PCF afterwards [8-14]. Unusual dispersive properties have been also observed in the fiber, so the ASPBGFs were often applied to femtosecond laser and amplifier developments [15-17]. The concept of hybrid-guiding PCF, which uses both index- and bandgap-guiding mechanisms simultaneously, naturally emerges from that of the ASPBGFs. Very unique optical properties have been realized from the hybrid-guiding concept, which are, for example, one polarization is guided light by M-TIR but the other is by BG, or light is confined by M-TIR at long wavelengths but by BG at short wavelength [18,19]. A variety of designs have been proposed and demonstrated to bring them into reality. Also, calculations have been made to support the measured optical properties. However, most of the calculations explain their findings in the given PCF structure. There is no systematic analysis that has been made to predict the optical properties of guided modes between index- and bandgap-guidings.

*Corresponding author: sdlim@kriss.re.kr

Color versions of one or more of the figures in this paper are available online.

In this study, the optical properties of guided modes in a hybrid-guiding region were calculated and analyzed. The design and modeling of such hybrid-guiding PCF was made by replacing the air-holes with HRIM inserts layer by layer in order. The optical properties such as mode intensity profile, mode dispersion, optical birefringence, confinement loss, and chromatic dispersion during transition between index- and bandgap-guidings were discussed in particular. The optical properties were also compared to the two reference PCFs, index-guiding and bandgap-guiding PCFs. Calculation of such a transition is useful for (1) looking into the possibility of combining the advantages of the two guiding regimes and (2) anticipating the guiding properties of an asymmetric PCF such as side-polished fiber sensor/device elements.

## II. DESIGN AND MODELING

The design and modeling is made from a commercially available PCF (NKT photonics LMA-8). The cross-section of the PCF has six rings of air holes in a hexagonal lattice as shown in Fig. 1.

The geometrical parameters are also taken from the real PCF design, where the air-hole pitch (center-to-center distance between the nearest holes), the air-hole diameter, and the outer cladding diameter are 5.7 μm, 2.3 μm, and 125 μm, respectively. The PCF with the air-hole to pitch ratio of less than 0.41 has been known as an endless single-mode fiber with no higher-order mode cut-off. The PCF modeled here is the fiber that delivers only the fundamental mode at all wavelengths. Two kinds of reference PCFs, index-guiding and bandgap-guiding PCFs are set by assigning 1 and 1.485 to the refractive index of the air-holes, respectively. The selection of the refractive index of 1.485 for HRIM is due to the lowest confinement loss of the reference bandgap-guiding PCF. In this study, Ge-doped silica with a refractive index of 1.485 is assumed as the HRIM. The two references, index-guiding and bandgap-guiding PCFs are shown in Fig. 1(a) and Fig. 1(k), respectively. In Fig. 1 are also shown PCFs with different numbers of HRIM layers. Red filled circles indicate HRIM inserts, and black hollow circles air holes. The number of HRIM layer increases from (a) to (k) in order of 0, 1, 3, 5, 6, 6.5, 7, 8, 10, 12 and 13 layers. Full-vector plane wave method (PWM) was used to find the bandgap map [20, 21]. Full-vector finite element method (FEM) [22] with anisotropic perfectly matched layers (PMLs) attached to the outer boundary of the fiber [23, 24] is used to calculate the mode optical properties of all PCF types including the index-guiding, bandgap-guiding, and a hybrid guiding PCFs. The analysis on the optical properties of guided modes is carried out

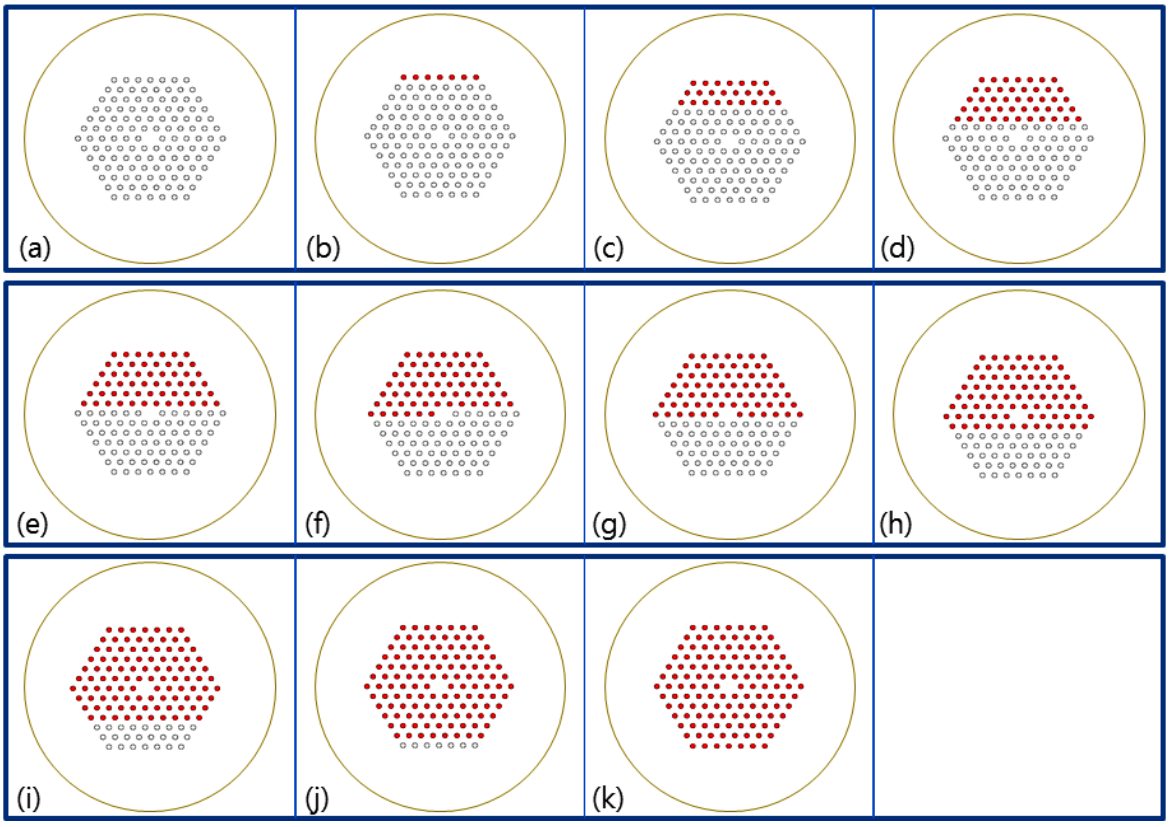


FIG. 1. Cross section of the PCF. Red filled circles denote HRIM inserts (n = 1.485), and black hollow circles denote air holes (n = 1). (a) to (k): 0, 1, 3, 5, 6, 6.5, 7, 8, 10, 12 and 13 layers of HRIM, respectively.

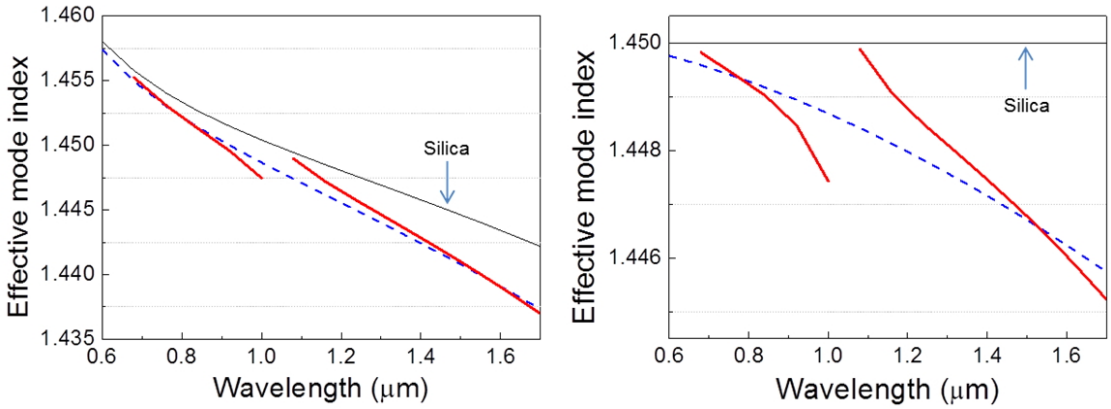


FIG. 2. (a) Total dispersion and (b) waveguide dispersion of index- and bandgap-guided modes. The black line represents the silica index. The index-guided and bandgap-guided modes are denoted by the blue dotted line and the red solid line, respectively.

based on the waveguide dispersion to concentrate on transition of the guiding mechanism, which is more clear when only the waveguide dispersion is taken into account. It is worth noting that the total dispersion can also be obtained simply by compensating for the difference of the material dispersion of silica if necessary. In order to verify it, the total dispersion is compared with the waveguide dispersion in Fig. 2.

The total dispersion shown in Fig. 2(a) is calculated by taking the material dispersion into account at each given wavelength. This is equivalent to that achieved by adding the difference between the actual silica index and 1.45 to the waveguide dispersion shown in Fig. 2(b).

## III. RESULTS AND DISCUSSION

Figure 3 shows the mode field profiles for the guided core modes in PCFs in the same order as in Fig. 1. The calculations are made at the wavelength of 1.4 μm in that the minimal confinement loss is observed in the 2nd bandgap region (1100 nm - 1700 nm, as will be shown in Fig. 7(b)).

Having the total index-guided and bandgap-guided modes (in Fig. 3(a) and in Fig. 3(k), respectively) compared, the bandgap-guided mode has a greater portion of energy in the cladding compared to the index-guided mode. This is obvious in the aspect that the light energy locates itself in higher index than lower one. In the same context, this verifies the known fact that the mode confinement by the photonic bandgap effect is generally weaker than that by the TIR. The calculation results also reveal that the mode field profiles in Figs. 3(b), 3(c), and 3(d) (group 1) are essentially the same as that of the index-guiding PCF. The mode field distributions in Figs. 3(h), 3(i), and 3(j) (group 2) show no significant difference from that of the bandgap-guiding PCF. The dispersion curves of the two mode groups are shown in Fig. 4.

The modes in each group share the identical dispersion curve within the uncertainty of our calculation. This means that the layers of HRIM have no influence on the dispersion of guided mode unless they are adjacent to the core. The bandgap-guided modes in group 2 are placed in the discrete photonic bandgaps (white region of Fig. 4). The 2nd and the 3rd bandgap regions appear over the wavelength range of our interest in Fig. 4.

However, the guided modes shown in Figs. 3(e), 3(f), and 3(g) are different from those of the two references. The modes have asymmetric field profiles toward the direction of the HRIM layers, exhibiting both the index-guiding and bandgap-guiding properties. These modes have been shown in the hybrid-guiding PCF. Figure 5 shows the dispersion of such guided modes in the hybrid-guiding region where both index-guiding and bandgap-guiding show themselves.

It is found from the calculation that the mode dispersion of the index-guiding PCF starts to be changed from the 6 layers of HRIM, exhibiting the bandgap-guiding properties. In the hybrid-guiding region, the mode dispersions locate in between those of the two reference fibers, where the modes undergo both index-guiding and bandgap-guiding confinement mechanisms at the same time. In the present case, the guided modes are confined by the bandgap effect at the top whereas by the M-TIR at the bottom as shown in the inset of Fig. 5. This transition is also illustrated in Figs. 3(e), (f), (g), and (h).

Figure 6 shows the optical birefringence of guided modes in the transition region as a function of wavelength.

The PCF modeled in this study has a hexagonal lattice structure (C6v symmetry), which has been known to have a circular symmetry as a circular-core step-index fiber [25]. Therefore, the PCF has no optical birefringence as the two reference fibers. However, the guided mode can experience a geometry-induced optical birefringence when the core is facing the layer of HRIM in part, which refers to the guided modes in the hybrid-guiding region. Asymmetricity in the refractive index profile around the core causes the optical birefringence between two eigen-states of polarization. The calculation results show that the PCFs with 6 and 7

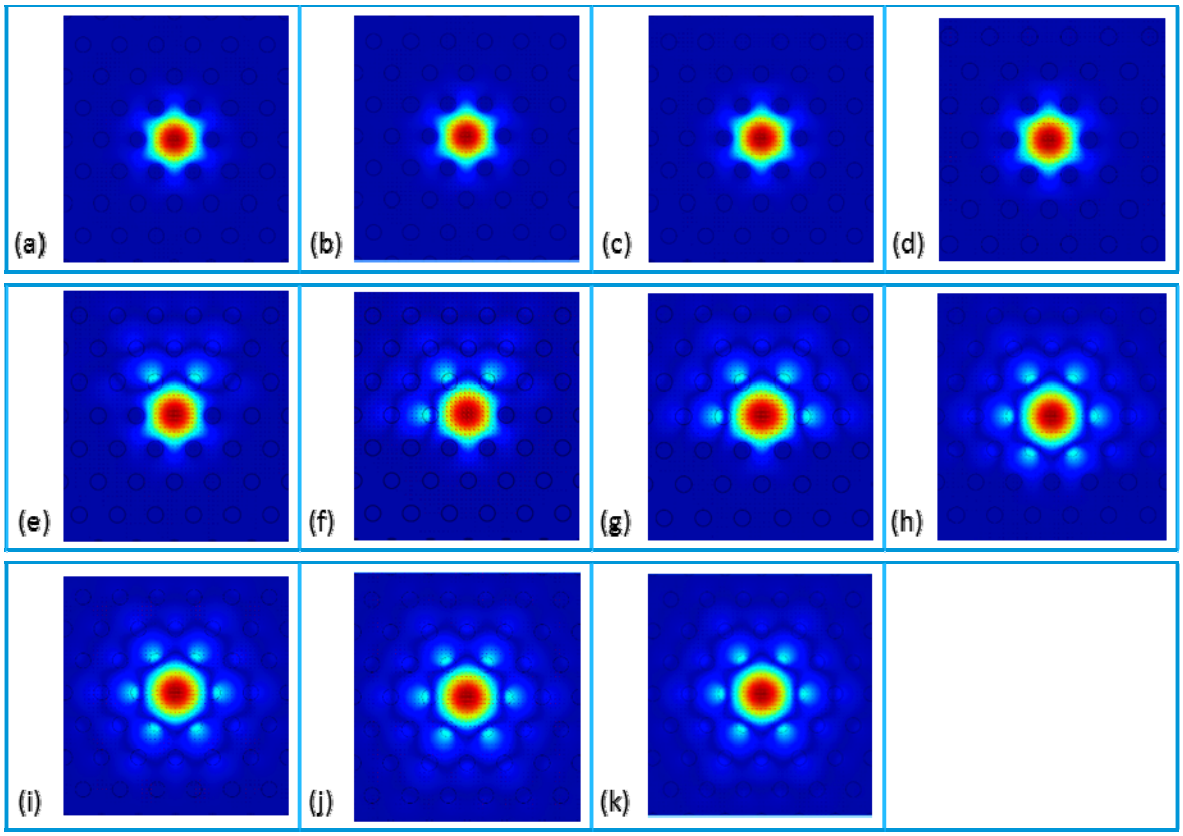


FIG. 3. Mode field profiles. (a), (b), …, and (k) correspond to the configurations of Fig. 1(a), Fig. 1(b), …, and Fig. 1(k), respectively.

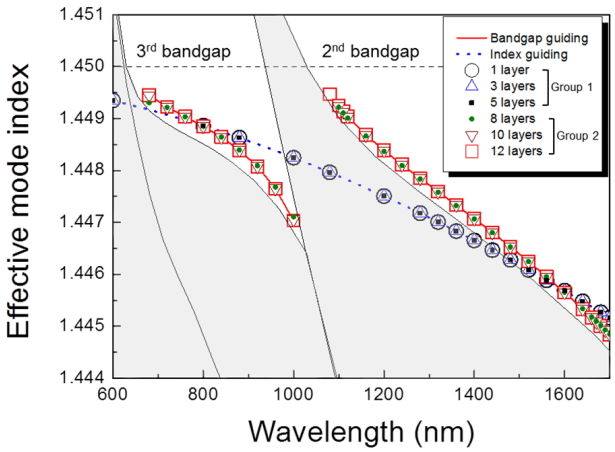


FIG. 4. Mode dispersions with respect to the number of HRIM layer. The black dashed line represents the silica index (n = 1.45). The index-guided and bandgap-guided modes are denoted by the blue dotted line and the red solid line, respectively. The 1, 3, and 5 layers and 8, 10, and 12 layers indicate the guided modes shown in Figs. 3(b), 3(c), and 3(d) (group 1) and Figs. 3(h), 3(i), and 3(j) (group 2), respectively.

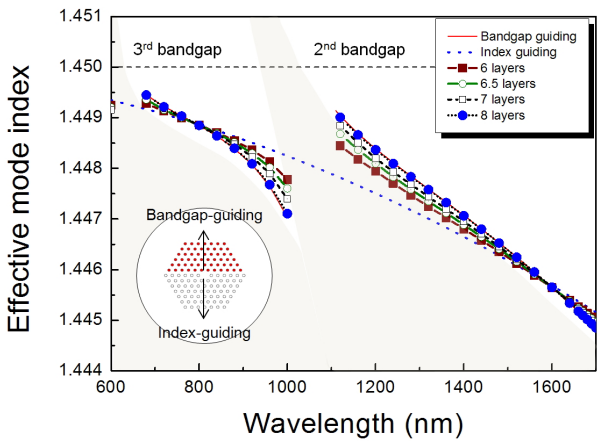


FIG. 5. Mode dispersion in hybrid-guiding region. The 6, 6.5, 7, and 8 layers represent the guided modes shown in Figs. 3(e), 3(f), 3(g), and 3(h), respectively.

layers of HRIM have the largest optical birefringence of $(3.0 \pm 0.2) \times 10^{-5}$. Noticeable finding here is that the PCF with 6.5 layers of HRIM has the lowest level of optical birefringence. In fact, the core surrounded by the 6.5 layers of HRIM has the refractive index profile that shows two-fold mirror anti-symmetry with respect to the angles of 30° and 120° from the horizontal axis as shown in the inset of Fig. 6. This cannot induce the optical form birefringence that has been created by the geometric asymmetricity [26]. The increase of the optical birefringence in the 2nd

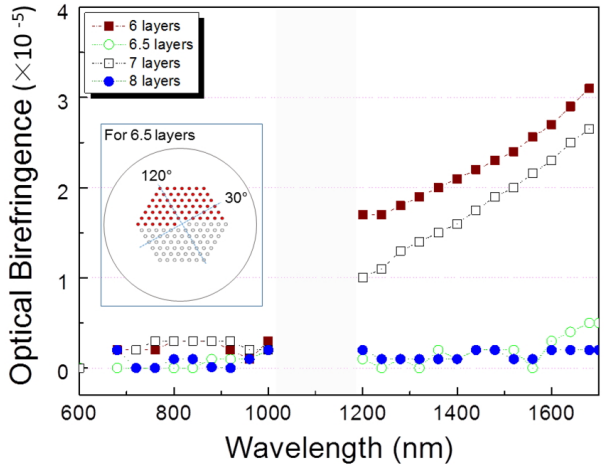


FIG. 6. Optical birefringence of guided modes in hybrid-guiding region. The 6, 6.5, 7, and 8 layers represent the guided modes shown in Figs. 3(e), 3(f), 3(g), and 3(h), respectively.

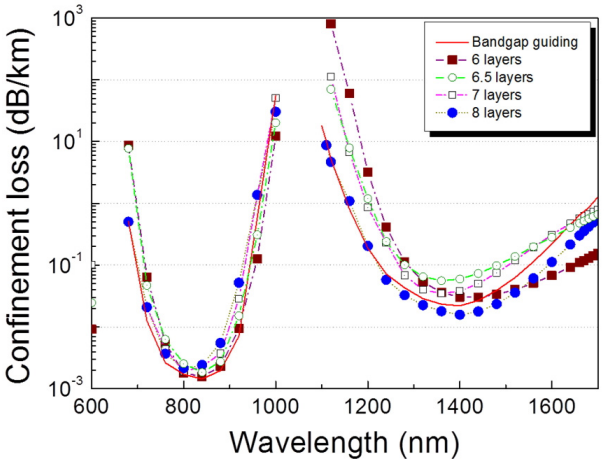


FIG. 7. Confinement loss of guided modes in hybrid-guiding region.

bandgap region is due to the fact that the difference between the core and cladding indices increases with wavelength, which results in higher optical birefringence for longer wavelength. In other words, this is because the mode field experiences the stronger asymmetricity at the longer wavelength. Figure 7 shows the confinement loss of the hybrid-guided modes as a function of wavelength.

The confinement loss in the hybrid-guiding region is almost identical to that of the bandgap-guiding PCF. One feature noticeable here is that the largest confinement loss is found for a PCF with 6 layers of HRIM in the 2nd bandgap region, and it decreases with the number of HRIM layers converging to that for bandgap-guiding PCF. It is worth noting that the confinement loss of the index-guiding PCF ranges from $10^{-11}$ dB/km at 600 nm to $10^{-8}$ dB/km at 1700 nm. It exponentially increases with the number of

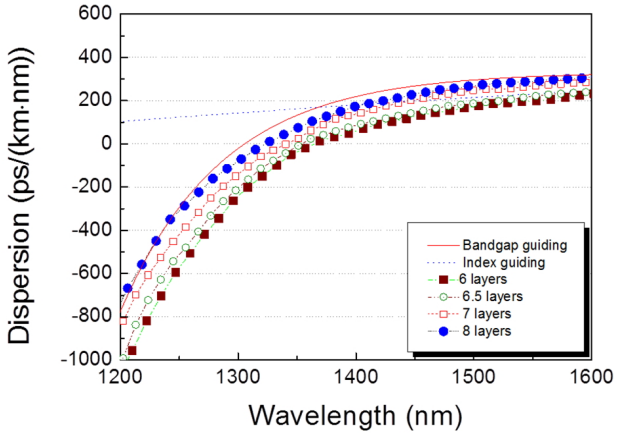


FIG. 8. Chromatic dispersion of guided modes in hybrid-guiding region over the 2nd bandgap of the reference bandgap-guiding PCF.

HRIM layer by a factor of 10 until the 6 layers of HRIM. Therefore, the confinement loss of $10^{-10}$ dB/km at 800 nm for the index-guiding PCF reaches up to $10^{-3}$ dB/km and $10^{-9}$ dB/km to $10^{-2}$ dB/km at 1400 nm. The exponential increase of the confinement loss with the number of HRIM layer indicates that the most outer air-hole ring involves in the mode confinement, and it can act as leakage channels by being replaced with HRIM.

The chromatic group delay dispersion of the hybrid-guided modes in the 2nd bandgap region is shown in Fig. 8.

The major finding is that the dispersion highly depends on the number of HRIM layers. The hybrid-guiding PCF can have even larger dispersion than those of both the index-guiding and the bandgap-guiding PCFs.

## IV. SUMMARY

We analyze the optical properties of the guided mode in a hybrid-guiding region where both the index-guiding and bandgap-guiding are valid. Numerical calculations are made in the PCF model with six rings of air holes in a hexagonal lattice. The hybrid-guiding PCF is designed by replacing the air holes with HRIM inserts layer by layer. Mode field profile, mode dispersion, optical birefringence, confinement loss, and chromatic dispersion are calculated and discussed. It is found that the mode dispersion locates between those of the index- and bandgap-guiding PCFs. The confinement losses of guided mode in the hybrid-guiding region are almost identical to that of the bandgap-guiding PCF. The guided modes in the hybrid-guiding region can have even larger chromatic dispersion than those of both the index-guiding and the bandgap-guiding PCFs. We believe such findings will be helpful to anticipate the optical properties of hybrid-guiding PCFs and to properly design optical devices using the PCFs.

## ACKNOWLEDGMENT

This work was supported by the Korea Research Institute of Standards and Science under the project 'Establishment of National Physical Measurement Standards and Improvements of Calibration/Measurement Capability,' and the R&D Convergence Program of NST (National Research Council of Science and Technology) of Republic of Korea (Grant No. CAP-15-08-KRISS).

## REFERENCES

1. P. Russell, "Photonic Crystal Fibers," Science **299**, 358-462 (2003).
2. T. A. Birks, J. C. Knight, and P. St. J. Russell, "Endlessly single-mode photonic crystal fiber," Opt. Lett. **22**, 961-963 (1997).
3. N. A. Mortensen, M. D. Nielsen, J. R. Folkenberg, A. Petersson, and H. R. Simonsen, "Improved large-mode-area endlessly single-mode photonic crystal fibers," Opt. Lett. **28**, 393-395 (2003).
4. T. A. Birks, D. Mogilevstev, J. C. Knight, and P. St. J. Russell, "Dispersion compensation using single-material fibers," IEEE Photon. Technol. Lett. **11**, 674-676 (1999).
5. A. Ortigosa-Blanch, J. C. Knight, W. J. Wadsworth, J. Arriaga, B. J. Mangan, T. A. Birks, and P. St. J. Russell, "Highly birefringent photonic crystal fibers," Opt. Lett. **25**, 1325-1327 (2000).
6. H. Ebendorff-Heidepriem, P. Petropoulos, S. Asimakis, V. Finazzi, R. C. Moore, K. Frampton, F. Koizumi, D. J. Richardson, and T. M. Monro, "Bismuth glass holey fibers with high nonlinearity," Opt. Express **12**, 5082-5087 (2004).
7. A. Ferrando, E. Silverstre, J. J. Miret, and P. Andrés, "Nearly zero ultraflattened dispersion in photonic crystal fibers," Opt. Lett. **25**, 790-792 (2000).
8. N. M. Litchinitser, S. C. Dunn, P. E. Steinvurzel, B. J. Eggleton, T. P. White, R. C. McPhedran, and C. M. de Sterke, "Application of an ARROW model for designing tunable photonic devices," Opt. Express **12**, 1540-1550 (2004).
9. C. Kerbage, P. Steinvurzel, P. Reyes, P. S. Westbrook, R. S. Windeler, A. Hale, and B. J. Eggleton, "Highly tunable birefringent microstructured optical fiber," Opt. Lett. **27**, 842-844 (2002).
10. L. Scolari, T. Alkeskjold, J. Riishede, A. Bjarklev, D. Hermann, Anawati, M. Nielsen, and P. Bassi, "Continuously tunable devices based on electrical control of dual-frequency liquid crystal filled photonic bandgap fibers," Opt. Express **13**, 7483-7496 (2005).
11. D. Yeom, P. Steinvurzel, B. J. Eggleton, S. D. Lim, and B. Y. Kim, "Tunable acoustic gratings in solid-core photonic bandgap fiber," Opt. Express **15**, 3513-3518 (2007).
12. S. A. Cerqueira, F. Luan, C. M. B. Cordeiro, A. K. George, and J. C. Knight, "Hybrid photonic crystal fiber," Opt. Express **14**, 926-931 (2006).
13. T. T. Larsen, A. Bjarklev, D. S. Hermann, and J. Broeng, "Optical devices based on liquid crystal photonic bandgap fibres," Opt. Express **11**, 2589-2596 (2003).
14. B. T. Kuhlmey, B. J. Eggleton, and D. K. C. Wu, "Fluid-Filled Solid-Core Photonic Bandgap Fibers," J. Lightwave Technol. **27**, 1617-1630 (2009).
15. A. Isomaki and O. G. Okhotnikov, "Femtosecond soliton mode-locked laser based on ytterbium-doped photonic bandgap fiber," Opt. Express **14**, 9238-9243 (2006).
16. A. Wang, A. K. George, and J. C. Knight, "Three-level neodymium fiber laser incorporating photonic bandgap fiber," Opt. Lett. **31**, 1388-1390 (2006).
17. V. Pureur, L. Bigot, G. Bouwmans, Y. Quiquempois, M. Douay, and Y. Jaouen, "Ytterbium-doped solid core photonic bandgap fiber for laser operation around 980 nm," Appl. Phys. Lett. **92**, 061113 (2008).
18. J. Sun and C. C. Chan, "Hybrid guiding in liquid-crystal photonic crystal fibers," J. Opt. Soc. Am. B **24**, 2640-2646 (2007).
19. M. Perrin, Y. Quiquempois, G. Bouwmans, and M. Douay, "Coexistence of total internal reflexion and bandgap modes in solid core photonic bandgap fibre with intersticial air holes," Opt. Express **15**, 13783-13795 (2007).
20. S. G. Johnson and J. D. Joannopoulos, "The MIT photonic-bands (MPB) package," http://ab-initio.mit.edu/wiki/index.php/MIT_Photonic_Bands.
21. S. G. Johnson and J. Joannopoulos, "Block-iterative frequency-domain methods for Maxwell's equations in a planewave basis," Opt. Express **8**, 173-190 (2001).
22. K. Saitoh and M. Koshiba, "Numerical Modeling of Photonic Crystal Fibers," J. Lightwave Technol. **23**, 3580-3590 (2005).
23. K. Saitoh and M. Koshiba, "Full-vectorial finite element beam propagation method with perfectly matched layers for anisotropic optical waveguides," J. Lightwave Technol. **19**, 405-413 (2001).
24. K. Saitoh and M. Koshiba, "Leakage loss and group velocity dispersion in air-core photonic bandgap fibers," Opt. Express **11**, 3100-3109 (2003).
25. M. Koshiba and K. Saitoh, "Structural dependence of effective area and mode field diameter for holey fibers," Opt. Express **11**, 1746-1756 (2003).
26. T. Ritari, H. Ludvigsen, M. Wegmuller, M. Legré, N. Gisin, J. R. Folkenberg, and M. D. Nielsen, "Experimental study of polarization properties of highly birefringent photonic crystal fibers," Opt. Express **12**, 5931-5939 (2004).